Available online at www.sciencedirect.com
SCIENCE DIRECT®
Journal of Organometallic Chemistry 689 (2004) 2808–2819
Journal of Organometallic Chemistry
www.elsevier.com/locate/jorganchem

Cu(I) and Ag(I) complexes of chalcogenide derivatives of the organometallic ligand dppf and the dppa analogue

Huizhang Liu [a], Nuno A.G. Bandeira [a], Maria José Calhorda [a,b,*], Michael G.B. Drew [c], Vitor Félix [d], Josef Novosad [e], Fabrizia Fabrizi de Biani [f], Piero Zanello [f]

[a] *Instituto de Tecnologia Química e Biológica (ITQB), Av. da República, EAN, Apt 127, 2781-901 Oeiras, Portugal*
[b] *Departamento de Química e Bioquímica, Faculdade de Ciências da Universidade de Lisboa, 1749-016 Lisboa, Portugal*
[c] *School of Chemistry, University of Reading, Whiteknights, Reading RG6 6AD, UK*
[d] *Departamento de Química, CICECO, Universidade de Aveiro, 3810-193 Aveiro, Portugal*
[e] *Department of Inorganic Chemistry, Faculty of Science, Masaryk University, Kotlárska 2, 611 37 Brno, Czech Republic*
[f] *Chemistry Department, University of Siena, Via Aldo Moro, I-43100, Italy*

Received 29 April 2004; accepted 10 June 2004

Abstract

New Cu(I) and Ag(I) complexes were prepared by reaction of $[M(NCCH_3)_4][X]$ (M = Cu or Ag; X = BF_4 or PF_6) with the bidentate chalcogenide ligands $Ph_2P(E)NHP(E)Ph_2$ (E = S, S_2dppa; E = Se, Se_2dppa), and dpspf (1,1′-bis(diphenylselenophosphoryl)ferrocene). Copper and silver behaved differently. While three molecules of either S_2dppa and Se_2dppa bind to a distorted tetrahedral Cu_4 cluster, with deprotonation of the ligand, 1:2 complexes of the neutral ligands are formed with Ag(I), with a tetrahedral coordination of the metal. The $[Cu_4\{Ph_2P(Se)NP(Se)Ph_2\}_3]^+$ clusters assemble as dimers, held together by weak Se···Se distances interactions. Another dimer was observed for the $[Ag(dpspf)]^+$ cation, with two short Ag···Se distances. DFT and MP2 calculations indicated the presence of attracting interactions, reflected in positive Mayer indices (MI). The electrochemistry study of this species showed that both oxidation and reduction took place at silver.

Keywords: Cu(I) complexes; Ag(I) complexes; Crystal structures; Clusters; DFT calculations; Electrochemistry

1. Introduction

Many Cu(I) and Ag(I) complexes of bidentate ligands have structures with the ligands in a chelate or in a bridging mode, and some of them exhibit interesting properties, such as luminescence [1]. Great interest in Cu(I) dimers has arisen from their biological role as oxygen carriers in proteins, such as haemocyanin, or as oxygen binders in cytochrome oxidase [2]. Bidentate phosphines, such as dppa ($Ph_2PNHPPh_2$) or dppm ($Ph_2PCH_2PPh_2$) often form binuclear species of the d^{10} Cu, Ag and Au cations containing an eight-membered cycle, where two ligands bridge the metals, and different numbers of axial coligands can also be present [3–5]. These ions usually adopt low coordination numbers, varying from linear to tetrahedral environments, [6] and more rarely to five-coordination [7]. Metal–metal bonds are also frequent in these compounds, the range of observed distances suggesting variations from strong to weak bonds or alternatively no interactions. The chalcogenide derivatives of the bidentate phosphines give rise to very different compounds, as described in previous publications [8–10]. One of them consists of a linear arrangement around the metal, as

* Corresponding author. Tel.: +351-214469754; fax: +351-214411277.
E-mail address: mjc@itqb.unl.pt (M.J. Calhorda).

0022-328X/$ - see front matter © 2004 Elsevier B.V. All rights reserved.
doi:10.1016/j.jorganchem.2004.06.012

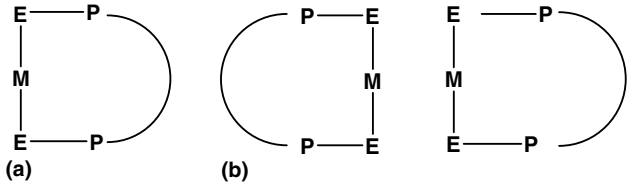

Scheme 1.

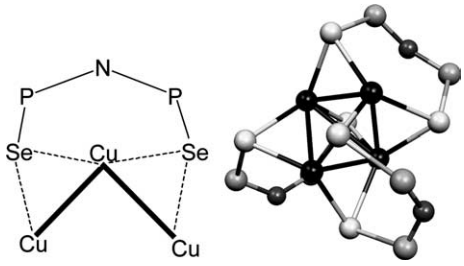

Scheme 2.

depicted in Scheme 1(a). It has been observed for the group 11 complexes of 1,1′-bis(diphenylthiophosphoryl)ferrocene (dptpf) [9,10a]. These units may assemble as in Scheme 2(b), being held by weak M···M interactions.

Tetrahedral coordination environments have also been obtained for Ag(I) and Au(I) with certain ligand combinations [8,10b], and the formation of tetrahedral clusters of Ag(I) has also been reported [10c].

In this work, M(I) cationic precursors (M = Cu, Ag) were used to prepare new derivatives of $Ph_2P(E)NHP(E)Ph_2$ (E = S, S_2dppa; E = Se, Se_2dppa), dptpf (1,1′-bis(diphenylthiophosphoryl)ferrocene) and its selenium analogue, dpspf. While Cu(I) tended to form tetrahedral clusters, and the ligand lost one proton, Ag(I) behaved very differently, affording mononuclear species or weakly bound dimers (Scheme 1). Their redox behaviour was studied by cyclic voltammetry, and DFT [11] and MP2 [12] calculations were performed in order to rationalize some experimental findings.

2. Results and discussion

2.1. Chemical studies

The reaction of the complex $[Cu(NCCH_3)_4][BF_4]$, in dichloromethane, under nitrogen, with the bis(diphenyl)phosphinoaminechalcogenide ligands, S_2dppa or Se_2dppa, 1:1, gave rise to similar white solids, which precipitated from the solution. They were characterized by single crystal X-ray diffraction (see details below), performed on crystals grown by slow diffusion of hexane into CH_2Cl_2 solutions of the material, and shown to be the tetrahedral clusters $[Cu_4\{Ph_2P(E)NP(E)Ph_2\}_3][BF_4]$(E = S, **1**; E = Se, **2**). While the amine protons are not observed on the X-ray structure, the stoichiometry is consistent with their loss, the ligand being deprotonated. The IR spectrum of the sulphur copper cluster **1** showed a band at 694 cm^{-1} that can be assigned to the $\nu_{P=S}$ vibration, shifted relative to that of the free ligand (622, 645 cm^{-1}) [13]. A similar band is observed at 687 cm^{-1} for the Se derivative, **2** (546, 595 in the free ligand) [14]. The ^1H NMR spectra are not very informative, as the only protons in the structure are those from the phenyl groups of the ligands. They are observed, in $NCCD_3$, as multiplets, between 7.18 and 7.98 δ (**1**), and 6.98 and 8.13 δ (**2**). The ^{31}P NMR spectra show a broad peak for the P atom of the ligand, at 27.05 δ (**1**), and 17.85 δ (**2**), but the resolution is low and no splittings are observed. They are shifted from the values of the free ligand, at 56.2 δ (S_2dppa) and 52.9 δ (Se_2dppa), respectively.

The reaction of $[Ag(NCCH_3)_4][BF4]$ in similar conditions (1:2 ratio) afforded the corresponding mononuclear complexes. Their structure, obtained by single crystal X-Ray diffraction, consisted of a tetrahedral Ag(I) complex with two chelating E_2dppa ligands $[Ag(E_2dppa)_2][BF_4]$ (E = S, **3**; E = Se, **4**). Although the cationic Se derivative had been prepared before [8], the presence of different counter-ions leads to different crystal structures (see details below). The IR spectra show peaks which can be assigned to the $\nu_{P=S/Se}$ vibration, at 689 cm^{-1} for **3** and at 687 cm^{-1} for **4**. The ^1H NMR spectra of the silver complex **3** in $NCCD_3$ exhibits a broad peak assigned to the H(N) proton, at 6.38 δ, and two broad peaks at 7.52 and 7.81 δ, corresponding to the phenyl protons. The Se analogue, **4**, has a similar spectrum, with broad peaks at 7.21 and 7.39 δ (protons of phenyl groups), while the H(N) proton appears at 3.67 δ. The phenyl protons have chemical shifts close to those reported in [8] (7.39, 7.88 δ, CD_2Cl_2), but the amine proton is more affected by the change in solvent.

The reaction of dpspf with $[M(NCCH_3)_4][PF_6]$ (M = Cu or Ag), in dichloromethane, gave rise to orange (Cu, **5**) or red (Ag, **6**) solids, with very similar spectroscopic data. The IR spectra are almost superimposable and show peaks which can be assigned to the $\nu_{P=Se}$ vibration, at 559 cm^{-1} for the copper derivative and at 557 cm^{-1} for the silver one. The P atom peak from the ligand in the ^{31}P NMR spectrum is seen at 29.58 δ (Cu), and 30.89 δ (Ag), respectively, but satellites are not easily observed. The ^1H NMR spectra of the copper complex **5** in $NCCD_3$ displays the multiplets of the phenyl protons at 7.43–7.63 δ and two doublets at 4.65–4.66 δ and 4.27–4.28 δ, which can be assigned to the four protons of the Cp ring in the ferrocenyl group. This pattern is also observed for the silver complex **6**, where the multiplets from the phenyl protons are found at 7.56–7.70 δ, and the Cp protons at 4.09 δ and 4.66–4.67 δ, the first appearing as a non-split peak. These

values suggest that the two complexes should have the same structure. Single crystal X-ray diffraction studies of the silver complex (see below) showed unequivocally the formation of a 1:1 species, [Ag(dpspf)][PF_6], **6**, represented in Scheme 1a, with two molecules assembling in dimers through short contact distances, as schematically depicted in Scheme 1b. Each molecule is equivalent to a monomeric analogue, [Ag(dpspf)][ClO_4], previously reported with a different counter-ion [9b].

The parallelism of the spectroscopic evidence and the elemental analysis support the same formulation for the copper complex, [Cu(dpspf)][PF_6], **5**. Pilloni et al. [9a] studied reactions of the same Cu(I) precursor with dpspf and the sulphur analogue, dptpf, and described the structure of the linear copper complex **5**.

2.2. Crystallography

The X-ray single crystal structures of four metal complexes of the chalcogenide dppa derivatives, namely two clusters [$Cu_4\{Ph_2P(S)NP(S)Ph_2\}_3$][$BF_4$], **1**, [$Cu_4\{Ph_2P(Se)NP(Se)Ph_2\}_3$][$BF_4$], **2**, and two mononuclear species [$Ag(S_2dppa)_2$][BF_4], **3**, and [$Ag(Se_2dppa)_2$][BF_4], **4**, were determined. The structures of the cations of **1** and **4** have been described before as $CuCl_2$ [15] or bromide [8] salts, respectively. However, they are reported here, since they offer the possibility to determine the influence of the counter-ion in the crystal packing of the cations $[Cu_4\{Ph_2P(S)NP(S)Ph_2\}_3]^+$ and $[Ag(S_2dppa)_2]^+$. Selected bond distances and angles are given in Table 1 for **1** and **2**, and in Table 3 for **3** and **4**.

The copper–sulphur cluster **1** crystallises in orthorhombic space group *Pbca*, while the copper–selenium cluster **2** crystallises in the triclinic space group $P\bar{1}$ and yields an asymmetric unit containing two complex cations $[Cu_4\{Ph_2P(Se)NP(Se)Ph_2\}_3]^+$, three BF_4^- anions, each with an occupancy of 0.666, and four water solvent molecules, three with occupancies of 0.333 and one with an occupation factor of 0.666. This formulation leads to the formula [$Cu_4\{Ph_2P(Se)NP(Se)Ph_2\}_3$][$BF_4$]·0.84$H_2O$. The charge balance of the molecular formulas of both complexes requires the imine groups to be deprotonated. A molecular diagram showing the overall structure and the spatial disposition of the two $[Cu_4\{Ph_2P(Se)NP(Se)Ph_2\}_3]^+$ units in the asymmetric unit of **2** is presented in Fig. 1.

The two independent cations of the asymmetric unit of **2**(a,b) are similar in their basic structures and geometric parameters (see Table 1). Three deprotonated $dppaSe_2$ ligands hold together four copper centres in a distorted tetrahedron environment, with Cu···Cu distances ranging from 2.761(3) to 2.873(3) Å, and

Table 1
Selected bond distances (Å) and angles (°) for complexes **1** and **2**

Complex **1**			
Cu(1)–Cu(2)	2.813(2)	Cu(1)–Cu(4)	2.781(2)
Cu(1)–Cu(3)	2.806(2)	Cu(2)–Cu(3)	2.791(2)
Cu(2)–Cu(4)	2.844(2)	Cu(3)–Cu(4)	2.773(2)
Cu(1)–S	2.266(2)–2.286(2)	Cu(2)–S	2.260(2)–2.291(2)
Cu(3)–S	2.288(2)–2.301(2)	Cu(4)–S	2.261(2)–2.279(2)
S–Cu–S	112.45(9)–124.04(9)	Cu–S–Cu	74.86(7)–77.07(8)
Cu–Cu–Cu	58.89(4)–61.47(4)	S–Cu–Cu	51.37(6)–53.22(6)
		S–Cu–Cu	102.15(7)–107.64(7)
Complex **2**			
Molecule 1			
Cu(1)–Cu(2)	2.832(3)	Cu(1)–Cu(3)	2.826(3)
Cu(1)–Cu(4)	2.761(3)	Cu(2)–Cu(3)	2.785(3)
Cu(2)–Cu(4)	2.873(3)	Cu(3)–Cu(4)	2.794(3)
Cu(1)–Se	2.385(2)–2.398(3)	Cu(2)–Se	2.359(2)–2.389(3)
Cu(3)–Se	2.377(2)–2.398(3)	Cu(4)–Se	2.355(2)–2.384(3)
Se–Cu–Se	115.3(1)–124.7(9)	Cu–Se–Cu	71.01(8)–74.23(8)
Cu–Cu–Cu	57.9(1)–62.0(7)	Se–Cu–Cu	52.6(1)–54.81(7)
		Se–Cu–Cu	101.95(9)–109.45(9)
Molecule 2			
Cu(5)–Cu(6)	2.812(3)	Cu(5)–Cu(7)	2.778(3)
Cu(5)–Cu(8)	2.841(3)	Cu(6)–Cu(7)	2.802(3)
Cu(6)–Cu(8)	2.783(3)	Cu(7)–Cu(8)	2.787(3)
Cu(5)–Se	2.349(3)–2.391(3)	Cu(6)–Se	2.368(3)–2.404(3)
Cu(7)–Se	2.373(3)–2.390(3)	Cu(8)–Se	2.358(3)–2.388(2)
Se–Cu–Se	115.7(1)–126.3(1)	Cu–Se–Cu	71.5(9)–73.7(9)
Cu–Cu–Cu	58.98(7)–61.38(7)	Se–Cu–Cu	52.54(7)–54.67(7)
		Se–Cu–Cu	103.0(1)–107.9(1)

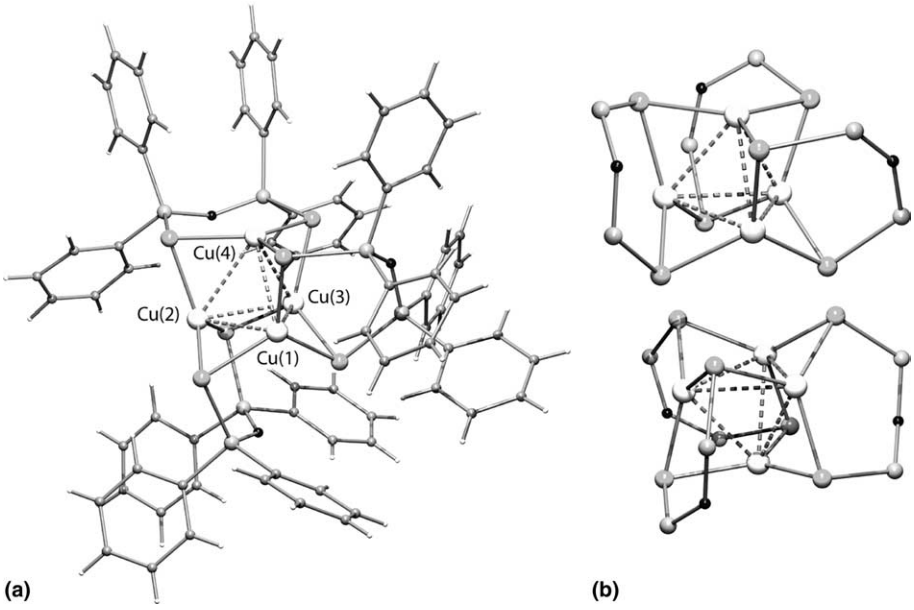

Fig. 1. Molecular diagrams of $[Cu_4\{Ph_2P(Se)NP(Se)Ph_2\}_3]^+$ **2**: (a) overall structure of the $[Cu_4\{Ph_2P(Se)NP(Se)Ph_2\}_3]^+$ cation. Only the copper centres are labelled for reasons of clarity. (b) $\{Cu_4\ (SePNPSe)_3\}^+$ core structures of two independent molecules present in the asymmetric unit, showing their spatial disposition.

2.778(3) to 2.841(3) Å, for molecules **a** and **b**, respectively. The angles Se–Cu–Se indicate that the selenium atoms are trigonally arranged around copper. The $dppaSe_2$ ligands act as bridging units, connecting different Cu atoms, or more precisely, connecting edges of the cluster (see Scheme 2 and Fig. 1).

Each copper centre is surrounded by selenium atoms from different bridges. Furthermore, the $\{Cu_4(SePNPSe)_3\}^+$ central unit displays an adamantane type structure, as shown in Fig. 1(b). The two independent units are self-assembled in such a way as to provide four short intermolecular Se···Se distances, ranging from 3.609(2) to 3.914(2) Å, which suggest some interactions between these molecules. This striking structural feature is apparent from Fig. 1(b) and will be recalled later. By contrast, the unique short Se···Se contact found within the Cu_4Se_4 clusters has a slightly longer distance of 3.933(2) Å.

To the best our knowledge, the structure of this complex is the first X-ray single crystal structure determination of a Cu_4Se_6 tetrahedral cluster reported in the literature, where the Se atoms belong to bidentate ligands. In fact, the $[Cu_4(\mu\text{-}SePh)_6]_6$ complex [16], was the unique tetranuclear copper cluster with a related structure found in the Cambridge Data Base [17]. Each of the six $SePPh_6$ ligands bridges two copper atoms over one edge of the tetrahedral core. The Cu···Cu distances are within the range found for **2**. The Cu–Se distances are slightly longer, between 2.371 and 2.426 Å, compared to 2.355(2)–2.398(3) Å in **2**. The M_4Se_6 adamantane type structural unit was also previously found in the silver tetrahedral cluster $[Ag_4\{Ph_2P(Se)NP(Se)Ph_2\}_3]^+$ [10]. The four silver centres are also linked by three deprotonated $dppaSe_2$ ligands, with Ag···Ag distances ranging from 2.989(1) to 3.310(1) Å. These are longer that those found for the copper cluster **2**, reflecting the different stereoelectronic sizes of Ag^+ and Cu^+ centres.

By contrast, the asymmetric unit of **1** comprises only one cluster cation $[Cu_4\{Ph_2P(S)NP(S)Ph_2\}_3]^+$ and one BF_4^-, and no short S···S intermolecular contacts were found in the crystal structure. The geometric parameters of $[Cu_4\{Ph_2P(S)NP(S)Ph_2\}_3]^+$ are similar to those found for this cation in $[Cu_4\{Ph_2P(S)NP(S)Ph_2\}_3][CuCl_2]$ [15], apart from the orientation of the phenyl groups, and consequently its structure is not discussed in detail here. In addition, these two structures are comparable to that described above for **2** and the Ag analogue [10c], the $\{Cu_4(SePN)_3\}^+$ core adopting also an adamantane arrangement. The values in Table 2 show the intramolec-

Table 2
Comparison of geometric parameters of Cu_4S_6 tetrahedral clusters having dithiolate bridging ligands

Ref. code	Cu···Cu range distances (Å)	⟨Cu–S⟩ (Å)
This work	2.773–2.844	2.280
DAHYUG	2.698–2.739	2.275
LISCOF	2.684–2.827	2.286
PPTICU20	2.763–2.814	2.267
SAKTON	2.671–2.732	2.280
VAMDES	2.717–2.789	2.267
YASWUK	2.663–2.801	2.666
YASXAR	2.652–2.747	2.264
YASXEV	2.729–2.740	2.274

ular Cu···Cu distances and the average Cu–S distances, found for BF_4^- (**1**) and $[CuCl_2]^-$ salts of the $[Cu_4\{Ph_2P(S)NP(S)Ph_2\}_3]^+$ cation (PPTICU20), and for other related Cu_4S_6 clusters having also thiolate ligands as binding units. The values are all very similar.

The crystal structures of the mono-nuclear complexes **3** and **4** are built in the triclinic space group $P\bar{1}$ and the asymmetric unit consists one complex cation, $[Ag(S_2dppa)_2]^+$ in **3** and $[Ag(Se_2dppa)_2]^+$ in **4** together with one BF_4^- anion. The molecular structure of $[Ag(S_2dppa)_2]^+$, **3**, together with the atomic notation scheme used is presented in Fig. 2. Distances and angles are given in Table 3.

The structure of the equivalent selenium derivative **4** is not shown. In each complex, the silver centre displays a distorted tetrahedral geometry with the angles subtended at the silver centre in the narrow range from 102.63(8)° to 117.25(9)° in **3**, and 97.98(9)° to 117.96(9)° in **4**. The S_2dppa and Se_2dppa ligands exhibit a chelating co-ordination mode forming six-membered chelated rings. In fact, these two complexes have quasi-"isomorphous" structures. The geometric parameters (bond distances and bond angles) involving the sulphur and selenium donors reflect the different stereo-electronic sizes of these atoms. Thus, the Ag–Se distances in **4** (2.634(2)–2.713(3) Å) are longer than the Ag–S distances in **3** (2.567(3)–2.604(3) Å) leading to an increase of 63 $Å^3$ in the unit cell volume of **4**. The remaining structural parameters within the dppa fragment are similar in both complexes. The P–N distances in both chelate rings of **3** and **4**, 1.685(7) and 1.677(6) Å in **3**, 1.673(13) and 1.703(15) Å in **4**, indicate single bonds between the phosphorus and the nitrogen atoms. The molecular dimensions of $[Ag(Sedppa)_2]^+$ in **4** are very similar to those reported for this cation in the bromide salt.

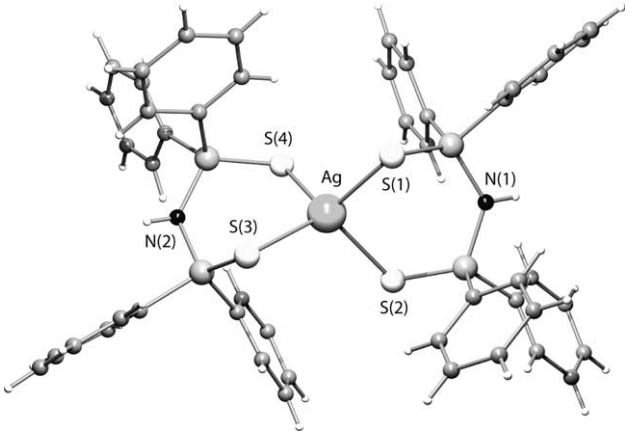

Fig. 2. Molecular diagram of the complex cation $[Ag(S_2dppa)_2]^+$, **3**, with the labelling scheme adopted.

Table 3
Selected bond distances (Å) and angles (°) for complexes **3** and **4**

Complex **3**			
Ag–S(1)	2.550(3)	Ag–S(3)	2.567(3)
Ag–S(4)	2.604(3)	Ag–S(2)	2.604(3)
S(1)–Ag–S(3)	110.30(9)	S(1)–Ag–S(4)	117.25(9)
S(3)–Ag–S(4)	106.43(9)	S(1)–Ag–S(2)	102.63(8)
S(3)–Ag–S(2)	117.25(9)	S(4)–Ag–S(2)	103.27(9)
Complex **4**			
Ag–Se(1)	2.713(3)	Ag–Se(2)	2.634(2)
Ag–Se(3)	2.663(3)	Ag–Se(4)	2.692(3)
Se(2)–Ag–Se(3)	110.20(9)	Se(2)–Ag–Se(4)	117.46(9)
Se(3)–Ag–Se(4)	108.32(9)	Se(2)–Ag–Se(1)	104.85(8)
Se(3)–Ag–Se(1)	117.96(9)	Se(4)–Ag–Se(1)	97.98(9)

The charge balances of the molecular formula of **3** and **4** require the two imino groups to be protonated, in agreement with spectroscopic evidence given above. For both complexes the imino protons were included in the structure refinement in the calculated positions (see Section 6) and they are involved in hydrogen bonding interactions with the BF_4^- counter-ion. These hydrogen bonds result in the formation of a one-dimensional (1-D) N–H···F network along the [0 1 0] base vector with anions alternating with cations, as illustrated in Fig. 3 for complex **3**.

This supramolecular structure can be compared with those found for the related complexes $[Ag(Se_2dppa)_2]Br$, **4b**, and $[Ag(Se_2dppa)_2]Br\cdot 1.5EtOH$, **4c** [8], which also crystallise in the triclinic space group $P\bar{1}$ [8]. The first complex, **4b**, has a large asymmetric unit composed of eight complex cations and eight bromide anions.

However, the N–H protons are engaged in hydrogen bonding with the bromides forming 1-D chains, which assemble in a supramolecular structure analogous to that found in the crystal structures of the complexes **3** and **4**. In the crystal structure of the complex **4c**, the bromide anions interact with the hydroxyl group of a solvate ethanol molecule via O–H···Br hydrogen bonds. These units bridge the molecules of complex cations through N–H···Br and N–H···O hydrogen bonds and again 1-D supramolecular networks are formed. This comparison shows that the cations are the structural motifs that organise these crystal structures, since the N–H imino groups from dppa ligand units permit the establishment of intermolecular bridges with counter-ions, which may also include solvent molecules.

Single crystal X-ray diffraction for the silver complex showed unequivocally the formation of the dimer of $[Ag(dpspf)][PF_6]$, **6**, with short Ag···Se contact distances between monomers, as shown in Scheme 3.

Unfortunately, this compound in the solid state was composed of ca. 50% of crystal and ca. 50% of powder, and displayed a very poor diffraction pattern. Indeed, the image plate pictures taken from the X-ray diffraction pattern from different crystals showed that they have low degree of crystallinity. The final quality of the crystal structure is not good enough for publication

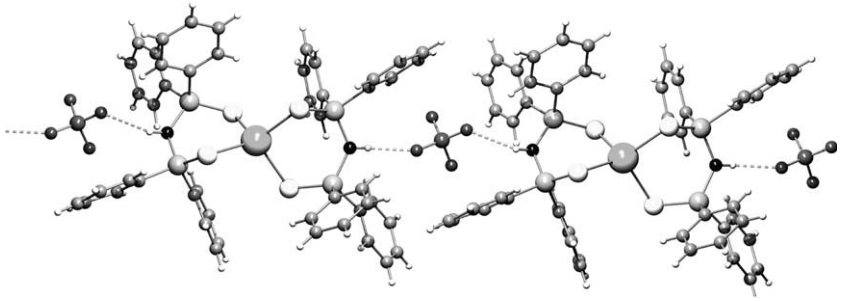

Fig. 3. View down the b crystallographic axis of the 1-D N–H···F network derived from molecular assembling of $[Ag(S_2dppa)_2]^{2+}$ cations and BF_4^- counter-ions in complex **3**.

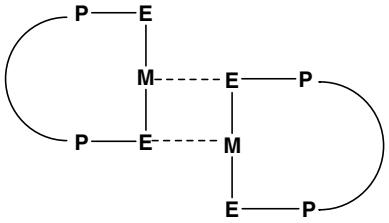

Scheme 3.

and prevents us from describing structural details in this work, although it seems likely that the monomer is equivalent to [Ag(dpspf)][ClO_4] [9b].

3. Electrochemistry

The interaction between the dpspf ligand and the coordinated silver ion in [**6**][PF_6] was investigated by electrochemical techniques. Due to the well known sensitivity to light of silver complexes, electrochemical experiments were performed in the dark.

Fig. 4(a) shows the cyclic voltammetric behavior of complex **6**[PF_6] in CH_3CN solution. It undergoes an irreversible anodic process at $E_p = +1.00$ V, ascribed to the Fe^{II}/Fe^{III} oxidation of the ferrocene fragment present in dpspf, which means that the corresponding monocation undergoes fast decomposition (no directly associated return peak has been detected even at 20 $V s^{-1}$). It also exhibits a reduction process at $E^{0'} = 0.00$ V, possessing features of chemical reversibility. In reality, at low scan rates the current ratio i_{pa}/i_{pc} is lower than unity (for example: $i_{pa}/i_{pc} = 0.7$ at 0.2 $V s^{-1}$), indicating that the reduction process is accompanied by slow chemical complications. Assuming the occurrence of a first-order side reaction, a lifetime $t_{1/2}$ of 3–4 s can be assigned to the Ag(0) complex [Ag(dpspf)] [18].

As Fig. 4(b) illustrates, a roughly similar behaviour has been observed in CH_2Cl_2 solution. At variance with the redox path in CH_3CN solution, the reduction process ($E_p = -0.19$ V) is complicated by fast following chemical reactions, evidenced also by the appearance

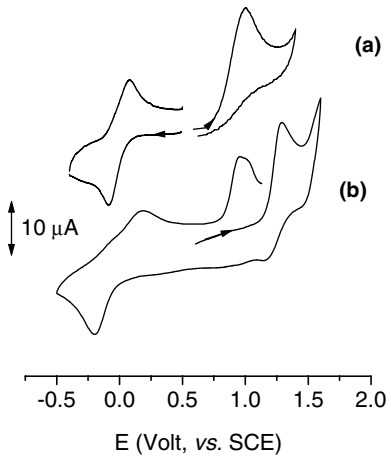

Fig. 4. Cyclic voltammograms recorded at a platinum electrode on: (a) CH_3CN solution containing [NEt_4][PF_6] (0.1 mol dm^{-3}) and **6** (1.2×10^{-3} mol dm^{-3}); (b) CH_2Cl_2 solution containing [NBu_4][PF_6] (0.2 mol dm^{-3}) and **6** (1.0×10^{-3} mol dm^{-3}). Scan rates 0.2 $V s^{-1}$.

of the anodic stripping peak ($E_p = +1.05$ V) of the electrodeposited metallic silver. Under these experimental conditions, however, the ferrocene based oxidation ($E^{0'} = +1.23$ V) is accompanied by a slower degradation of the corresponding monocation. As a matter of fact the lifetime of $[Ag(dpspf)]^{2+}$ can be roughly evaluated to be less than 1 s.

4. Molecular orbital calculations

The two $[Cu_4\{Ph_2P(Se)NP(Se)Ph_2\}_3]^+$ units in the crystal structure of **2** assemble in such a way that there are close contacts between Se atoms (from 3.62 to 4.34 Å). Also, the $[Ag(dpspf)]^+$ cation (**6**) was found to be a dimer with two short Ag···Se distances, although it had been observed as a monomer in a previous study, where the counter-ion was different [9b]. We performed DFT [11] (ADF program [19]) and MP2 [12] calculations, when possible, in order to study the weak interactions between the two closed shell systems. As both systems are considerably large, the phenyl groups were replaced

by hydrogen atoms, in order to build a reasonably sized model. The silver dimer was studied in more detail, owing to the shorter contact inter units and the smaller number of atoms. The geometry of the models of both the dimer (**m6**) and the monomer (**m6m**) were fully optimised, under C_i symmetry and no symmetry, respectively (DFT calculations, ADF program; more details in Section 6). The structure obtained from the X-ray single crystal diffraction is shown in Fig. 5(a), and the calculated one in Fig. 5(b). The structure of the monomer in **m6** (**m6m**) can be compared with the published one [9b], and, despite the poor quality, with that of the monomer shown in Fig. 5(a), since the positions of the heavy atoms Se and Ag should be reliable.

The Se–Ag–Se arrangement varies significantly. It is apparent from Fig. 5 that the presence of the bulky phenyl groups influences the behavior of the central group. The Ag–Se distances, quoted as 2.453(3) Å in [9b], become slightly different (2.573, 2.575 Å) in **m6**, but very different in **6** (2.450 and 2.497). This asymmetrization is associated with the formation of the dimer, since each silver atom tends toward becoming three coordinated. The third intermolecular Ag···Se contact is 3.438 or 2.925 Å, in **6** and **m6**, and the Se–Ag–Se decreases from 176.5(1)° in [9b], to 176.4° in the calculated **m6**, and 162° in **6**. The P–Se bonds in the optimized structure **m6** have the same length (2.178 Å), longer than the average value of 2.132(6) Å given in [9b]; in **6**, however, the distances are longer and different (2.158 and 2.178 Å), probably reflecting the asymmetric environment created by the packing of the bulky phenyl groups when organized in the close vicinity of the dimer. Since distances are not always good indicators of bond formation, Mayer indices MI [20], were calculated, for dimers and their monomers, as reported in Table 4, while the assignment of bonds is given in Scheme 4.

The MIs vary according to the bond lengths, becoming larger as the bond gets shorter, and indicate that the Ag···Se intermolecular contacts can be considered as weak bonds. When the monomer, with the same geometry it has in the dimer, is considered (**6m** or **m6m**) the

Table 4
Mayer indices for the Ag–Se and P–Se bonds in the optimized structure (ADF) of **m6** and in the experimental structure **6**

Bond	6[a]	6m	m6	m6m
a	0.672	0.656	0.649	0.638
b	0.573	0.656	0.526	0.617
c	0.266	–	0.305	–
d	1.337	1.335	1.345	1.359
e	1.282	1.335	1.267	1.349

[a] Coordinates from the experimental structure with phenyl groups replaced by hydrogens.

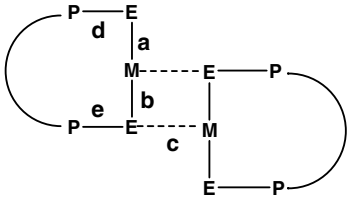

Scheme 4.

MIs for the two Ag–Se bonds are almost the same. This shows that, when Se forms this extra bond **c**, one of the initial Ag–Se bond, **b**, becomes weaker, as expected. The intermolecular bond is formed at the expense of the intramolecular ones. The effect of dimer formation on the P–Se bond is attenuated and the two bonds do not become significantly different, although they are more symmetric in the monomer.

If indeed there is a dimer, where the two monomers are held by the two weak Ag–Se bonds, the binding energy can be calculated. It can be done in two different ways: ΔE_1 can be defined as the difference between the energy of the dimer and twice the energy of the monomer with the same geometry as it has in the dimer; if the monomers are allowed to relax, the difference ΔE_2 between the energy of the dimer and twice the energy of the optimized monomer is considered. ΔE_1 was calculated as 24.7 kcal mol^{-1}, indicating a repulsive interaction. The values of ΔE_2 are much more repulsive, since the relaxation energy of two

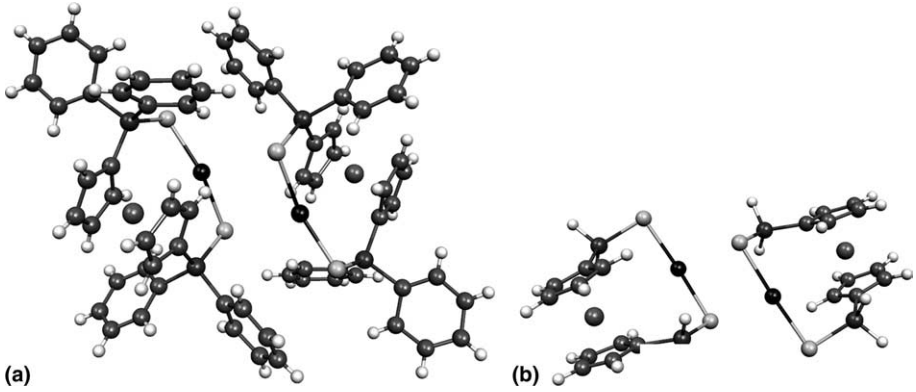

Fig. 5. The structure of the [Ag(dpspf)]$^+$ cation **6** (a) and the calculated structure of the model **m6** (b).

monomers has to be introduced. The interaction energy involved ΔE_1 (24.7 kcal mol^{-1}) may eventually be overcome by cation–anion electrostatic and crystal packing forces. It is reasonable to assume that changing the counter-ion from perchlorate to hexafluorophosphate may induce the dimerization of the Ag complex, as the interactions between cation and anion described in [9b] are replaced by interaction between cations and between these cations and anions.

However, since DFT methods are not particularly suited for detecting weak closed shell interactions [21], MP2 calculations were performed in a smaller model, obtained by replacing the ferrocenylphosphine by PH_2 (**sm6**). The geometry of the new dimer model was optimized and the calculated MIs, as well as ΔE_1, are given in Table 5.

The data concerning the Ag–Se and P–Se bonds are similar to what has been described above, except for the Ag···Se intermolecular index of 0.096, which reflects a weaker interaction. The interaction energy ΔE_1 is still positive, meaning that the interaction is still repulsive.

For comparison, we also performed ADF calculations on this small model. The results parallel those obtained for the larger models (Table 4), but the repulsion is larger. It appears that correlation effects, taken into account more efficiently by the MP2 calculation, play some role in holding together the monomers. On the other hand, the energy calculated for the smaller models is more repulsive, suggesting that in the real dimer the situation may become more favourable.

The copper cluster **2** is larger and the possibility of running calculations is even more limited. We carried out (ADF) a complete structure optimization of a model of the dimer (**2m**), where all the phenyl groups were replaced by hydrogen atoms. The optimized geometry is shown in Fig. 6. The bonds between the selenium atoms and copper are not shown for clarity. The selenium atoms bridge over edges of the tetrahedral cluster, forming two triangles, above a Cu3 face of each cluster, resulting in a stacking of four layers Cu3–Se3–Se3–Cu3 (Fig. 6). On the opposite side, there is a concentration of hydrogen atoms (phenyl groups in the experimental structure). The calculated binding energy for this dimer is 24 kcal mol^{-1} (repulsive). This result is not surprising in view of the preceding discussion of the silver dimer. Also in this case, the large number of phenyl groups may significantly contribute to packing forces, which help to stabilize the dimeric structure.

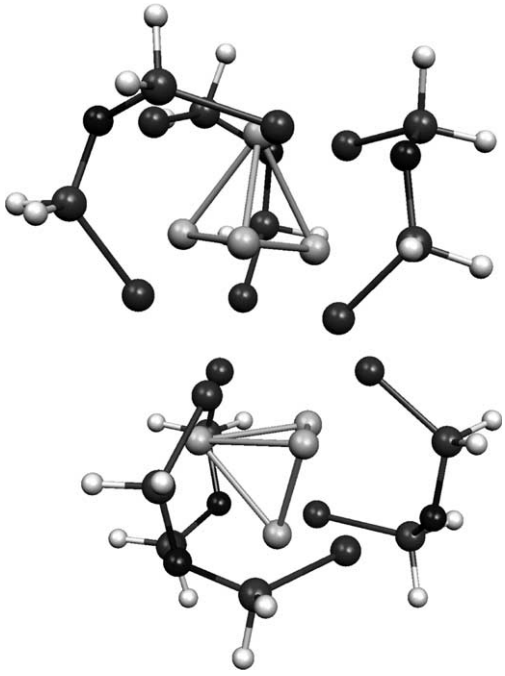

Fig. 6. Optimized geometry (ADF) of a model (**m2**) of the dimeric species **2**.

We also calculated MIs to check whether any weak interaction took place between the selenium atoms defining the two triangles facing each other (Fig. 6). The shortest distances are 3.4–3.5 Å, but most are longer (4.16–4.19 Å), becoming as long as the Se···Se distances inside each triangle.

The calculated MIs are all small, the largest (0.017, 0.031) corresponding to the shortest distances. Also attractive, but even smaller, interactions are detected between some Se atoms inside each triangle.

Table 5
Mayer indices for the Ag–Se and P–Se bonds in the optimized structure of the small model **sm6** (MP2 and ADF) and in their monomers (**sm6m**), and the respective binding energy ΔE_1 (kcal mol^{-1})

Bond	MP2		ADF	
	sm6	**sm6m**	**sm6**	**sm6m**
a	0.694	0.635	0.659	0.635
b	0.562	0.654	0.491	0.589
c	0.096	–	0.331	–
d	1.172	1.191	1.325	1.354
e	1.152	1.190	1.281	1.353
ΔE_1	27.6		31.1	

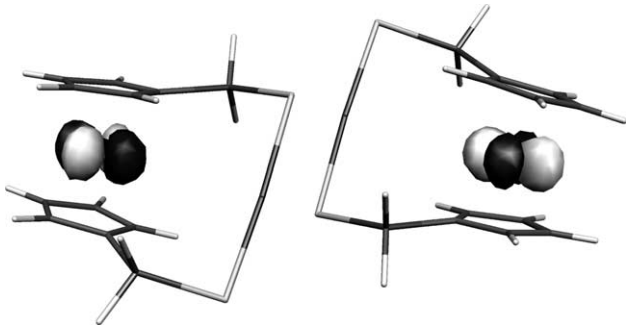

Fig. 7. DFT calculated HOMO of the model **m6** in a Molekel representation [22].

The frontier orbitals of the model of the silver complex (**m6**) confirm the interpretation of the oxidation process in the electrochemistry studies. Indeed, the HOMO is mainly a non bonding orbital localized on iron, as depicted on Fig. 7.

5. Conclusions

The $[M(NCCH_3)_4]^+$ cations (M = Cu or Ag) react differently with $Ph_2P(E)NHP(E)Ph_2$ ligands (E = S or Se). Ag(I) formed tetrahedral complexes with two molecules of the ligand and Cu(I) induced the deprotonation of the ligand and gave rise to distorted tetrahedral copper $[Cu_4\{Ph_2P(E)NP(E)Ph_2\}_3]^+$ clusters. The Se and S clusters differ in their crystal structure, as short Se···Se contacts between units are observed in the former, while the S atoms of the latter are shielded from those of adjacent clusters by the phenyl groups. Mayer indices obtained from DFT calculations showed the existence of weak Se···Se bonds. The selenium derivative of the ferrocenyl type ligand binds in a 1:1 fashion to both Cu and Ag. In the Ag complex, two units interact through formation of intermolecular Ag–Se bonds, also characterized by their MIs, in an arrangement not observed in the crystal structure of the perchlorate derivative. These bonds were studied in detail using several models and both DFT and MP2 calculations.

6. Experimental

6.1. Syntheses

Commercially available reagents and all solvents were purchased from standard chemical suppliers. All solvents were used without further purification except acetonitrile (dried over CaH_2) and dichloromethane (dried over CaH_2). The complexes $[M(NCCH_3)_4][X]$ and (M = Cu or Ag; X = BF_4 or PF_6) were synthesised according to the literature procedures [23,24]. The preparation of the ligands S_2dppa, Se_2dppa and dpspfSe_2 is based on existing synthetic routes [25–27].

^{1}H NMR spectra were recorded on a Bruker AMX-300 (300 MHz) spectrometer in d^3CD_3CN (δ 1.93), using TMS as internal reference, and ^{31}P shifts were measured with respect to external 85% H_3PO_4. Elemental analyses were carried out at ITQB. The IR spectra were recorded on a Unicam Mattson 7000 FTIR spectrometer. Samples were run as KBr pellets.

6.2. *$[Cu_4\{Ph_2P(S)NP(S)Ph_2\}_3][BF_4]$*, **1**

A solution of dppaS_2 (90 mg, 0.2 mmol) in CH_2Cl_2 (5 ml) at room temperature was added to a solution of $[Cu(NCCH_3)_4][BF_4]$ (74 mg, 0.23 mmol) in CH_2Cl_2 (5 ml) under an atmosphere of nitrogen. The solution was stirred for 1 h, hexane was added and a white powder precipitated. The precipitate was filtered off, washed several times with small amounts of hexane, and dried in vacuum. Yield: 0.070 g (72%).

Single crystals (cubic, colourless) suitable for X-ray diffraction were obtained by diffusion of hexane into a concentrated CH_2Cl_2 solution of the product.

Found (calculated for $Cu_4S_6P_6C_{72}H_{60}N_3BF_4$): C, 48.02 (51.27); H, 3.57 (3.59); N, 2.29 (2.49); S, 10.81 (11.41)%. NMR (CD_3CN, ppm): ^{1}H, 7.18–7.92 (m, 20H, C_6H_5). ^{31}P, 27.05. IR (KBr, cm^{-1}): 694($\nu_{P=S}$).

6.3. *$[Cu_4\{Ph_2P(Se)NP(Se)Ph_2\}_3][BF_4]$*, **2**

A solution of dppaSe_2 (109 mg, 0.2 mmol) in CH_2Cl_2 (5 ml) at room temperature was added to a solution of $[Cu(NCCH_3)_4][BF_4]$ (74 mg, 0.23 mmol) in CH_2Cl_2 (5 ml) under an atmosphere of nitrogen. The solution was stirred for 1 h, hexane was added and a white powder precipitated. The precipitate was filtered off, washed several times with small amounts of hexane, and dried in vacuum. Yield: 0.090 g (79%).

Single crystals (cubic, colourless) suitable for X-ray diffraction were obtained by diffusion of hexane into a concentrated CH_2Cl_2 solution of the product.

Found (calculated for $Cu_4Se_6P_6C_{72}H_{60}N_3BF_4$): C, 38.06 (43.95); H, 3.03 (3.07); N, 1.74 (2.13)%. NMR (CD_3CN, ppm): ^{1}H, 6.98–8.13 (m, 20H, C_6H_5). ^{31}P, 17.85. IR (KBr, cm^{-1}): 687($\nu_{P=Se}$).

6.4. *$[Ag(dppaS_2)_2][BF_4]$*, **3**

A solution of dppaS_2 (90 mg, 0.2 mmol) in CH_2Cl_2 (5 ml) at room temperature was added to a solution of $[Ag(NCCH_3)_4][BF_4]$ (42 mg, 0.12 mmol) in CH_2Cl_2 (5 ml) under an atmosphere of nitrogen. The solution was stirred for 1 h, hexane was added and a white powder precipitated. The precipitate was filtered off, washed several times with small amounts of hexane, and dried in vacuum. Yield: 0.080 g (62%).

Single crystals (colourless) suitable for X-ray diffraction were obtained by diffusion of hexane into a concentrated CH_2Cl_2 solution of the product.

Found (calculated for $AgS_4P_4C_{48}H_{40}N_2BF_4$): C, 47.50 (52.81); H, 3.74 (3.69); N, 2.14 (2.57); S, 11.03 (11.75)%. NMR (CD_3CN, ppm): ^{1}H, 7.52–7.81 (m, 20H, C_6H_5). ^{31}P, 33.00. IR (KBr, cm^{-1}): 689($\nu_{P=S}$).

6.5. *$[Ag(dppaSe_2)_2][BF_4]$*, **4**

A solution of dppaSe_2 (109 mg, 0.2 mmol) in CH_2Cl_2 (5 ml) at room temperature was added to a solution of $[Ag(NCCH_3)_4][BF_4]$ (42 mg, 0.12 mmol) in CH_2Cl_2 (5 ml) under an atmosphere of nitrogen. The solution was stirred for 1 h, hexane was added and a white

powder precipitated. The precipitate was filtered off, washed several times with small amounts of hexane, and dried in vacuum. Yield: 0.090 g (60%).

Single crystals (colourless) suitable for X-ray diffraction were obtained by diffusion of hexane into a concentrated CH_2Cl_2 solution of the product.

Found (calculated for $AgSe_4P_4C_{48}H_{40}N_2BF_4$): C, 39.67 (45.07); H, 3.24 (3.15); N, 2.03 (2.19)%. NMR (CD_3CN, ppm): ^1H, 7.19–7.39 (m, 20H, C_6H_5). ^{31}P, 21.46. IR (KBr, cm^{-1}): 687($\nu_{P=Se}$).

6.6. [Cu(dpspf)][PF$_6$], 5

Solid dpspf (143 mg, 0.2 mmol) was added to a solution of $[Cu(NCCH_3)_4][PF_6]$ (74 mg, 0.2 mmol) in CH_2Cl_2 (10 ml) under an atmosphere of nitrogen at room temperature. The solution was stirred for about 1 h, hexane was added, and a yellow–brown powder precipitated. The precipitate was filtered off, washed several times with small amounts of hexane, and dried in vacuum. Yield: 0.140 g (76%).

Single crystals (yellow–brown needles) suitable for X-ray diffraction were obtained by vapour diffusion of Et_2O into a concentrated $(CH_3)_2CO$ solution of the product.

Found (calculated for $CuFeSe_2P_3C_{34}H_{28}F_6$): C, 44.15 (44.35); H, 3.26 (3.06)%. NMR (CD_3CN, ppm): ^1H, 7.43–7.63 (m, 20H, C_6H_5); 4.65–4.66 (m, 2H, C_5H_4); 4.27–4.28 (m, 2H, C_5H_4). ^{31}P, 29.58. IR (KBr, cm^{-1}): 559 ($\nu_{P=Se}$).

6.7. [Ag(dpspf)][PF$_6$], 6

Solid dpspf (143 mg, 0.2 mmol) was added to a solution of $[Ag(NCCH_3)_4][PF_6]$ (74 mg, 0.2 mmol) in CH_2Cl_2 (10 ml) under an atmosphere of nitrogen at room temperature. The solution was stirred for about 1 h, hexane was added, and a yellow–brown powder precipitated. The precipitate was filtered off, washed several times with small amounts of hexane, and dried in vacuum. Yield: 0.150 g (78%).

Single crystals (red needles) suitable for X-ray diffraction were obtained by diffusion of hexane into a concentrated CH_2Cl_2 solution of the product.

Found (calculated for $AgFeSe_2P_3C_{34}H_{28}F_6$): C, 39.1 (42.31); H, 2.68 (2.92)%. IR (KBr, cm^{-1}): 557.5 (ν_{P-Se}). NMR (CD_3CN, ppm): ^1H, 7.56–7.70 (m, 20H, C_6H_5); 4.09 (s, 2H, C_5H_4); 4.66–4.67 (m, 2H, C_5H_4). ^{31}P, 30.89. IR (KBr, cm^{-1}): 557 ($\nu_{P=Se}$).

6.8. Crystallography

A summary of the crystallographic data, together with data collection and the refinement details for $[Cu_4\{Ph_2P(S)NP(S)Ph_2\}][BF_4]$ **1**, $[Cu_4\{Ph_2P(Se)NP(Se)Ph_2\}][BF_4]\cdot 0.84H_2O$, **1**, **2**, $[Ag(S_2dppa)_2][BF_4]$, **3**, and $[Ag(Se_2dppa)_2][BF_4]$, **4**, is given in Table 6.

X-ray data sets for these four complexes were collected on a MAR research image plate system equipped with graphite-monochromated Mo Kα radiation (0.71073 Å). Ninety five frames were measured at 2° intervals using a counting time adequate to the crystal under study. Data analyses were performed with XDS program [28]. Empirical absorption corrections were applied to the intensities of complexes **2** and **4** using the DIFABS program [29]. The positions of the heavy atoms were obtained using direct methods and the positions of remaining non-hydrogen atoms appeared subsequently on successive difference Fourier maps. The structures of **1**, **3** and **4** were refined by full-matrix least-squares

Table 6
Room temperature crystal data and pertinent refinement details for complexes **1**–**4**

Complex	1	2	3	4
Formula	$C_{72}H_{60}BCu_4F_4N_3P_6S_6$	$C_{72}H_{61.33}B_{1.50}Cu_4F_6N_3OP_6Se_6$	$C_{48}H_{21}AgBF4N2P_4S_4$	$C_{48}H_{21}AgBF4N2P_4Se_4$
M_w	1686.38	2028.53	1092.63	1281.24
Crystal System	Orthorombic	Triclinic	Triclinic	Triclinic
Space group	*Pbca*	$P\bar{1}$	$P\bar{1}$	$P\bar{1}$
a (Å)	20.336(27)	18.944(19)	10.068(11)	10.101(13)
b (Å)	23.196(27)	24.816(26)	15.159(17)	15.414(17)
c (Å)	32.069(35)	19.334(23)	16.665(18)	16.845(19)
α (°)	(90.0)	90.14(1)	105.25(1)	106.33(1)
β (°)	(90.0)	94.99(1)	93.59(1)	93.63(1)
γ (°)	(90.0)	90.30(1)	90.70(1)	90.71(1)
V (Å^3)	15127.4	9054.5	2447.9	2510.6
Z	8	4	2	2
D_c (mg m^{-3})	1.481	1.488	1.482	1.695
μ (mm^{-1})	1.455	3.495	0.765	3.479
Reflections collected	50003	16359	7696	5427
Unique reflections, (R_{int})	14761, (0.0834)	16359	7696	5427
Final *R* indices				
$R_1wR_2[I>2\sigma I]$	0.0958, 0.2525	0.0865, 0.2560	0.0956, 0.2660	0.1016, 0.3126
R_1wR_2 (all data)	0.1430, 0.2867	0.1347, 0.2935	0.1836, 0.3161	0.1754,0.3819

against F^2. The refinement of the structure of **2** was performed by block-diagonal least-squares. The C–H hydrogen atoms were inserted in idealised positions and allowed to refine, riding on the parent C atom with an isotropic thermal parameter equal to 1.2 times those to which they were bonded. In complexes **3** and **4** the N–H hydrogen atoms were retrieved from last difference Fourier maps and included in refinement with N–H distances constrained to 0.86 Å given also $U_{iso} = 1.2\ U_{eq}$. Anisotropic thermal were used for all non-hydrogen atoms, except the B and F atoms from BF_4^- anions, oxygen atoms of water molecules in complex **2**, which were refined with isotropic temperature factors. These species and found to be disordered were refined using the disorder model described above. The B–F and F···F distances were constrained in order to give an ideal tetrahedral geometry.

All calculations required to solve and refine the structures were carried out with SHELXS and SHELXL from the SHELX97 package [30]. Molecular diagrams were drawn with PLATON graphical software [31].

6.9. Electrochemistry

Measurements were performed in dichloromethane or acetonitrile solutions containing $[NBu_4][PF_6]$ (0.2 mol dm^{-3}) and $[NEt_4][PF_6]$ (0.1 mol dm^{-3}) supporting electrolytes, respectively. Anhydrous 99.8% acetonitrile and anhydrous 99.9%, HPLC grade dichloromethane were purchased from Aldrich. Electrochemical grade $[NEt_4][PF_6]$ and $[NBu_4][PF_6]$ were purchased from Fluka. Cyclic voltammetry was performed in a three-electrode cell containing a platinum working electrode surrounded by a platinum-spiral counter electrode, and an aqueous saturated calomel reference electrode mounted with a Luggin capillary. A BAS 100W electrochemical analyser was used as polarising unit. All the potential values are referred to the saturated calomel electrode (SCE). Under the present experimental conditions, the one-electron oxidation of ferrocene occurs at $E^{0'} = +0.39$ V (in CH_2Cl_2) and +0.38 V (in CH_3CN), respectively.

6.10. Computational details

Density functional calculations [11] were carried out with the Amsterdam Density Functional program (ADF-2002) [19]. The local spin density (LSD) exchange correlation potential was used with the local density approximation of the correlation energy (Vosko, Wilk and Nusair's) [32]. Gradient corrected geometry optimizations [33], without symmetry constraints, were performed using the generalized gradient approximation (Becke's nonlocal exchange [34] and Perdew's correlation corrections [35]. A triple-ζ Slater-type orbital (STO) basis set augmented by two polarization functions was used for Se; triple-ζ STO basis set augmented by one polarization function were used for Cu, Ag, Fe, and N; double-ζ STO basis set augmented by one polarization function were used for P, C, and H. A frozen core approximation was used to treat the core electrons: (1s) for N and C; ([1–2]s, 2p) for P, Cu, and Fe; ([1–3]s [2–3]p 3d) for Ag and Se. The models were based on the crystal structures described above, with the phenyl groups replaced by hydrogen atoms.

The PC-GAMESS package [36,37] was used to run MP2 calculations. Geometry optimizations were carried out with the Los Alamos double-ζ pseudopotential [38]. Additional p and d functions were added to the standard basis set for selenium, and an additional f function [39] was added for silver; standard Pople triple-ζ segmented 6-311G(p,d) basis sets [40], were used for the lighter elements (P and H). No symmetry constraints were imposed on the models built as described in the text, except for the larger Ag dimers, **6m** (C_i). Bond orders as defined by Mayer [20] were calculated at the energy minima.

7. Supplementary material

The crystal structures have been deposited at the Cambridge Crystallographic Data Centre and allocated the deposition numbers: **1** 23,7504; **2** 23,7505; **3** 23,7506; **4** 23,7507.

Acknowledgement

H.L. thanks Praxis XXI for a postdoctoral grant. V.F. thanks FCT for a sabbatical leave grant. M.J.C. and P.Z. gratefully acknowledge the financial support of ICCTI and CNR (in the frame of the Cooperative Programme 2001/2002) and P.Z. the financial support of the University of Siena (PAR 2003). J.N. thanks the Ministry of Education of the Czech Republic (MSM 143100011) for the financial support and NATO Fellowship (ICCTI – 01157 22/02/99). The University of Reading and EPSRC are thanked for funds for the Image Plate system. We thank Zara Miravent Tavares for the elemental analysis (ITQB).

References

[1] (a) P.C. Ford, E. Cariati, J. Bourassa, Chem. Rev. 99 (1999) 3625; (b) V.W.-W. Yam, W.K.-M. Fung, K.-K. Cheung, Angew. Chem.,Int. Ed. Engl. 35 (1996) 1100.
[2] J.J.R. Fraústo da Silva, R.J.P. Williams, The Biological Chemistry of the Elements, Clarendon Press, Oxford, 1991.

[3] (a) S. Kitagawa, H. Maruyama, S. Wada, M. Munukata, M. Nakamura, H. Masura, Bull. Chem. Soc. Jpn. 64 (1991) 2809;
(b) M. Maekawa, M. Munukata, S. Kitagawa, T. Kuroda-Sowa, Y. Suenaga, M. Yamamoto, Inorg. Chim. Acta 271 (1998) 129.
[4] (a) J.D. Basil, H.H. Murray, J.P. Fackler Jr., J. Tocher, A.M. Mazany, B. Trzcinska-Bancroft, H. Knachel, D. Dudis, T.J. Delord, D.O. Marler, J. Am. Chem. Soc. 107 (1985) 6908;
(b) H. Schmidbaur, Gold Bull. 23 (1990) 11;
(c) H. Schmidbaur, Pure Appl. Chem. 65 (1993) 691.
[5] (a) L.F. Veiros, M.J. Calhorda, J. Organomet. Chem. 510 (1996) 71;
(b) M.J. Calhorda, L.F. Veiros, J. Organomet. Chem. 478 (1994) 37.
[6] (a) B.W. Smucker, K.R. Dunbar, J. Chem. Soc., Dalton Trans. (2000) 1309;
(b) G. Pilloni, B. Corain, M. Degano, B. Longato, G. Zanotti, J. Chem. Soc., Dalton Trans. (1993) 1777;
(c) H. Börzel, P. Comba, K.S. Hagen, C. Katsichtis, H. Pritzkow, Chem. Eur. J. 6 (2000) 914.
[7] H. Liu, M.J. Calhorda, M.G.B. Drew, V. Félix, J. Novosad, L.F. Veiros, F. Fabrizi de Biani, P. Zanello, J. Chem. Soc., Dalton Trans. (2002) 4365.
[8] J.D.E.T. Wilton-Ely, A. Schier, H. Schmidbaur, J. Chem. Soc., Dalton Trans. (2001) 3647.
[9] (a) G. Pilloni, B. Longato, G. Bandoli, B. Corain, J. Chem. Soc., Dalton Trans. (1997) 819;
(b) G. Pilloni, B. Longato, G. Bandoli, Inorg. Chim. Acta 298 (2000) 251.
[10] (a) M.C. Gimeno, P.G. Jones, A. Laguna, C. Barroca, J. Chem. Soc., Dalton Trans. (1995) 3563;
(b) S. Canales, O. Crespo, M.C. Gimeno, P.G. Jones, A. Laguna, J. Organomet. Chem. 613 (2000) 50;
(c) S. Canales, O. Crespo, M.C. Gimeno, P.G. Jones, A. Laguna, A. Silvestru, C. Silvestru, Inorg. Chim. Acta 347 (2003) 16.
[11] R.G. Parr, W. Yang, Density Functional Theory of Atoms and Molecules, Oxford University Press, New York, 1989.
[12] (a) C. Møller, M.S. Plesset, Phys. Rev. 46 (1934) 618;
(b) J.S. Binkley, J.A. Pople, Int. J. Quantum Chem. 9 (1975) 229;
(c) J.S. Binkley, J.A. Pople, R. Seeger, Int. J. Quantum Chem. S 10 (1976) 1;
(d) R. Krishnan, J.A. Pople, Int. J. Quantum Chem. 14 (1978) 91;
(e) R. Krishnan, M. Frisch, J.A. Pople, J. Chem. Phys. 72 (1980) 4244.
[13] J.P. Mcquillan, I.A. Oxton, Inorg. Chim. Acta 29 (1978) 69.
[14] P. Bhattacharya, J. Novosad, J. Phillips, A.M.Z. Slavin, D.J. Williams, J.D. Woollins, J. Chem. Soc., Dalton Trans. (1995) 1607.
[15] C.P. Huber, M.L. Post, O. Siiman, Acta Cryst. B 34 (1978) 2629.
[16] X. Jin, K. Tang, Y. Long, Y. Tang, Acta Cryst. Sect. C 55 (1999) 1799.
[17] (a) F.H. Allen, Acta Cryst. B 58 (2002) 380;
(b) I.J. Bruno, J.C. Cole, P.R. Edginton, M. Kessler, C.F. Macrae, P. McCabe, J. Pearson, R. Taylor, Acta Cryst. B 58 (2002) 389.
[18] E.R. Brown, J.R. Sandifer, in: B.W. Rossiter, J.F. Hamilton (Eds.), Physical Methods of Chemistry, Electrochemical Methods, vol. 2, Wiley, New York, 1986 (Chapter 4).
[19] (a) ADF-2002, E.J. Baerends, A. Bérces, C. Bo, P.M. Boerrigter, L. Cavallo, L. Deng, R.M. Dickson, D.E. Ellis, L. Fan, T.H. Fischer, C. Fonseca Guerra, S.J.A. van Gisbergen, J.A. Groeneveld, O.V. Gritsenko, F.E. Harris, P. van den Hoek, H. Jacobsen, G. van Kessel, F. Kootstra, E. van Lenthe, V.P. Osinga, P.H.T. Philipsen, D. Post, C.C. Pye, W. Ravenek, P. Ros, P.R.T. Schipper, G. Schreckenbach, J.G. Snijders, M. Sola, D. Swerhone, G. te Velde, P. Vernooijs, L. Versluis, O. Visser, E. van Wezenbeek, G. Wiesenekker, S.K. Wolff, T.K. Woo, T. Ziegler;
(b) C. Fonseca Guerra, O. Visser, J.G. Snijders, G. te Velde, E.J. Baerends, Parallelisation of the Amsterdam density functional programme, in: E. Clementi, C. Corongiu (Eds.), Methods and Techniques for Computational Chemistry, STEF, Cagliari, 1995, pp. 303–395;
(c) C. Fonseca Guerra, J.G. Snijders, G. te Velde, E.J. Baerends, Theor. Chem. Acc. 99 (1998) 391;
(d) E.J. Baerends, D. Ellis, P. Ros, Chem. Phys. 2 (1973) 41;
(e) E.J. Baerends, P. Ros, Int. J. Quantum Chem. S 12 (1978) 169;
(f) P.M. Boerrigter, G. te Velde, E.J. Baerends, Int. J. Quantum Chem. 33 (1988) 87;
(g) G. te Velde, E.J. Baerends, J. Comp. Phys. 99 (1992) 84.
[20] (a) I. Mayer, Int. J. Quantum Chem. 29 (1986) 73;
(b) Mayer 1.0.8 by Chris Empson. Available from <http://freeside.dcs.hull.ac.uk/~ch8cje/mayer/index.php>.
[21] (a) P. Pyykkö, Chem. Rev. 97 (1997) 597;
(b) P. Pyykkö, N. Runerberg, F. Mendizabal, Chem. Eur. J. 3 (1997) 1451;
(c) N. Runerberg, M. Schütz, H.-J. Werner, J. Chem. Phys. 110 (1999) 7210;
(d) F.A. Cotton, X. Feng, J. Am. Chem. Soc. 119 (1997) 7514;
(e) K. Andersson, C.W. Bauschlicher Jr., B.J. Persson, B.O. Roos, Chem. Phys. Lett. 257 (1996) 238.
[22] S. Portmann, H.P. Lüthi, Chimia 54 (2000) 766.
[23] G.J. Kubas, Inorg. Synth. 29 (1979) 90.
[24] R.B. King, J.J. Eisch (Eds.), Organometallic Synthesis, vol. 3, Elsevier, Amsterdam, 1986, p. 316.
[25] F.T. Wang, J. Najdzionek, K.L. Leneker, H. Wasserman, D.M. Braitsch, Synth. React. Inorg. Met.-Org. Chem. 8 (1978) 119.
[26] P. Bhattacharyya, J. Novosad, J. Phillips, A.M.Z. Slawin, D.J. Williams, J.D. Woollins, J. Chem. Soc., Dalton Trans. (1995) 1607.
[27] J.J. Bishop, A. Davison, J. Organometal. Chem. 27 (1971) 241.
[28] W. Kabsch, J. Appl. Crystallogr. 21 (1988) 916.
[29] N. Walker, D. Stuart, DIFABS, Acta Cryst. A 39 (1983) 158.
[30] G.M. Sheldrick, SHELX-97, University of Göttingen, Göttingen, Germany, 1997.
[31] A.L. Spek, PLATON, A Multipurpose Crystallographic Tool, Utrecht University, Utrecht, The Nederlands, 1999.
[32] S.H. Vosko, L. Wilk, M. Nusair, Can. J. Phys. 58 (1980) 1200.
[33] (a) L. Versluis, T. Ziegler, J. Chem. Phys. 88 (1988) 322;
(b) L. Fan, T.J. Ziegler, Chem. Phys. 95 (1991) 7401.
[34] A.D. Becke, Phys. Rev. A 38 (1988) 3098.
[35] J.P. Perdew, Phys. Rev. B 33 (1986) 8822.
[36] (a) A.A. Granovsky, Laboratory of Chemical Cybernetics, Moscow State University, Moscow, Russia, ©1994, 2004. Some parts of this program include code due to work of Jim Kress, Peter Burger and Robert Ponec. Available from <http://quantum-2.chem.msu.ru/gran/gamess/index.html>;
(b) M.W. Schmidt, K.K. Baldridge, J.A. Boatz, S.T. Elbert, M.S. Gordon, J.H. Jensen, S. Koseki, N. Matsunaga, K.A. Nguyen, S.J. Su, T.L. Windus, M. Dupuis, J.A. Montgomery, J. Comput. Chem. 14 (1993) 1347.
[37] PC-GAMESS version 6.4, build number 2555. M.W. Schmidt, K.K. Baldridge, J.A. Boatz, S.T. Elbert, M.S. Gordon, J.H. Jensen, S. Koseki, N. Matsunaga, K.A. Nguyen, S.J. Su, T.L. Windus, M. Dupuis, J.A. Montgomery, J. Comput. Chem. 14 (1993) 1347.
[38] C.E. Check, T.O. Faust, J.M. Bailey, B.J. Wright, T.M. Gilbert, L.S. Sunderlin, J. Phys. Chem. A 105 (2001) 8111. http://www.emsl.pnl.gov/forms/basisform.html .
[39] A.W. Ehlers, M. Böhme, S. Dapprich, A. Gobbi, A. Höllwarth, V. Jonas, K.F. Köhler, R. Stegmann, A. Veldkamp, G. Frenking, Chem. Phys. Lett. 208 (1993) 111.
[40] R. Krishnan, J.S. Binkley, R. Seeger, J.A. Pople, J. Chem. Phys. 72 (1980) 650.